Full waveform inversion using preserved amplitude reverse time migration

Botao Qin, Thibaut Allemand, Gilles Lambaré, CGG*

Summary

A great deal of effort has been expended to improve the amplitude reliability of migration. The similarity of reverse time migration (RTM) to the gradient of full waveform inversion (FWI) indicates that preserved amplitude RTM can help improve FWI. We develop the theoretical derivation of an improved gradient for FWI based on common shot preserved amplitude RTM. We validate our approach on the Marmousi II model and the Chevron SEG 2014 dataset, showing that it significantly improves the convergence rate of FWI.

Introduction

The connection between migration and the gradient of FWI was identified early in the history of FWI (Lailly, 1983; Tarantola, 1984). This connection is particularly valid concerning reflected waves but much less for diving waves. Indeed, while diving waves are generally muted in depth migration they are critical for the success of FWI (Pratt, 1999). This, in addition to the non-linear aspect of FWI, implies that FWI cannot fully reduce to a migration plus a stratigraphic inversion. We can, however, still find some interesting cross-fertilizations between them.

In migration, an aspect that has been studied in particular in the past has been amplitude preservation. Within ray+Born and ray+Kirchhoff approximations, accurate and efficient migration/inversion formulae have been proposed and adopted by the industry (Beylkin, 1985; Bleistein, 1987; Jin et al., 1992). More recently, these have been extended to wave equation migration (Zhang et al., 2007) and RTM (Zhang and Sun, 2009). Considering that RTM and FWI share the same wave modelling engine, can we take advantage of these approaches for FWI?

Zhang et al. (2014) proposed a first approach derived from angle domain preserved amplitude RTM, which allows to compute impedances and velocity perturbations. The use of angle domain RTM allows to separate impedance and velocity but also makes the method expensive in 3D (Xu et al., 2011; Duveneck, 2013), especially considering the iterative relaxation approach used by FWI.

As an alternative, easier to implement in 3D, we derive an improved expression of the FWI gradient based on a shot domain preserved amplitude RTM. Among other potential applications, we validate our approach for FWI.

We begin with a description of shot domain preserved amplitude RTM. We then derive the inversion formula to estimate the velocity perturbation based on the Born approximation. Next, we discuss potential applications of our approach, in particular describing how the method can be incorporated into an FWI workflow using reflected data to provide iterated velocity model updates. Finally, we show results from the Marmousi II dataset and the Chevron/SEG 2014 FWI blind test dataset to demonstrate that our approach can speed up the convergence relative to conventional FWI.

Theory

Let us consider a designatured shot record $d(x_r,y_r;t;\mathbf{x}_s)$ where (x_r,y_r) is the receiver position at the surface, t is time and $\mathbf{x}_s$ is the shot position. Common shot RTM (Zhang and Sun, 2009) consists in taking the zero time-lag cross-correlation of the forward and backward wavefields, p_F and p_B, respectively, namely:

$$R(\mathbf{x}) = \int dt\, p_F(\mathbf{x};t;\mathbf{x}_s)\, p_B(\mathbf{x};t;\mathbf{x}_s) \tag{1}$$

where $R(\mathbf{x})$ is the reflectivity and $\mathbf{x}$ the position in the migrated image. In the acoustic isotropic assumption the forward propagated source wavefield, p_F, satisfies:

$$\left(\frac{1}{v^2}\frac{\partial^2}{\partial t^2} - \rho\nabla\frac{1}{\rho}\cdot\nabla\right)p_F(\mathbf{x};t;\mathbf{x}_s) = \delta(\mathbf{x}-\mathbf{x}_s)\delta(t), \tag{2}$$

and the backward propagated receiver wavefield, p_B, satisfies:

$$\begin{cases}\left(\frac{1}{v^2}\frac{\partial^2}{\partial t^2} - \rho\nabla\frac{1}{\rho}\cdot\nabla\right)p_B(\mathbf{x};t;\mathbf{x}_s) = 0, \\ p_B(x,y,z=0;t;\mathbf{x}_s) = d(x,y;t;\mathbf{x}_s),\end{cases} \tag{3}$$

where $v = v(\mathbf{x})$ and $\rho = \rho(\mathbf{x})$ denote the velocity and the density, respectively.

The high frequency asymptotic expressions of p_F and p_B given in terms of source and receiver traveltimes and amplitudes are:

$$p_F(\mathbf{x};\omega;\mathbf{x}_s) = \frac{SA_s}{\sqrt{\rho}}e^{-i\omega\tau_s}, \tag{4}$$

and:

$$p_B(\mathbf{x};\omega;\mathbf{x}_s) = \int dx\, 2i\omega\frac{\partial\tau_r}{\partial z}\frac{\bar{S}A_r}{\sqrt{\rho}}d(x_r,y_r;t,\mathbf{x}_s)e^{i\omega\tau_r} \tag{5}$$

where $\tau_s = \tau_s(\mathbf{x};\mathbf{x}_s)$ and $\tau_r = \tau_r(\mathbf{x};\mathbf{x}_r)$ are the traveltimes from the source and receiver to the subsurface point, respectively; $A_s = A(\mathbf{x};\mathbf{x}_s)$ and $A_r = A(\mathbf{x};\mathbf{x}_r)$ are the amplitude of the Green's functions from the source and receiver to the subsurface point, respectively; $S = S(\omega)$ is the signature of the Green's function which depends on the dimension of the propagation; the bar over the function denotes complex conjugate.

DOI http://dx.doi.org/10.1190/segam2015-5865645.1

For a reference velocity, v_0, $\delta v(\mathbf{x}) = v - v_0$, denotes the velocity perturbation. For the case with no density perturbation, the perturbed wavefield, δp, satisfies the Born approximation:

$$\left(\frac{1}{v^2}\frac{\partial^2}{\partial t^2} - \rho\nabla\frac{1}{\rho}\cdot\nabla\right)\delta p(\mathbf{x};t;\mathbf{x}_s) = \frac{2\delta v}{v_0^3}\frac{\partial^2}{\partial t^2}p(\mathbf{x};t;\mathbf{x}_s) \tag{6}$$

Using the method developed by Beylkin (1985) or Bleistein et al. (2001), we can express the perturbed velocity model as a summation over the perturbed wavefield:

$$\delta v(\mathbf{x}) = \frac{2v_0}{\pi\rho}\iint dx_r d\omega \frac{\partial\tau_r}{\partial z}\cos^2\theta\frac{A_r^2}{G_s G_r}\delta p(\mathbf{x}_r;\omega;\mathbf{x}_s) \tag{7}$$

where $\theta = \theta(\mathbf{x}_s;\mathbf{x};\mathbf{x}_r)$ is the reflection angle; $G_s = G(\mathbf{x};\omega;\mathbf{x}_s)$ and $G_r = G(\mathbf{x};\omega;\mathbf{x}_r)$ are the Green's functions. We only present the formula in 3D.

Employing δp instead of the data record d in the backward propagation of RTM in equation (3), and substituting relations (4) and (5) into equation (7), we can rearrange equation (7) into the following inversion formula:

$$\delta v(\mathbf{x}) = \frac{v_0^3}{2\pi\rho}\int d\omega\frac{i}{\omega^3}\frac{\nabla p_B\cdot\nabla\overline{p}_F + p_B\nabla^2\overline{p}_F}{p_F\overline{p_F}}. \tag{8}$$

The denominator in (8) is the same as in the deconvolution imaging condition of RTM. It requires applying some stabilization (Guitton et al., 2007). In practice, we use:

$$p_F\overline{p_F} = \langle p_F\overline{p_F}\rangle + \varepsilon(\mathbf{x}), \tag{9}$$

where $\langle\ldots\rangle$ is a spatial smoothing operator with suitable smoothing windows, and ε is an additive damping factor which depends on the subsurface location.

Our approach is close to the one developed by Zhang et al. (2014), who in addition considered the case of a density perturbation. Except for this, the main difference is that our approach is based on a common shot RTM implementation which is simpler and less computational intensive than a common angle RTM.

Applications

The first straightforward application of our approach is FWI. Indeed, in conventional FWI (Tarantola, 1984) using the steepest descent method, at each iteration the velocity is updated in the gradient direction of the least-squares cost function:

$$E(\delta v) = \|\delta p(\mathbf{x}_r;t;\mathbf{x}_s)\|^2. \tag{10}$$

We propose to modify this standard implementation of FWI by replacing the gradient direction with the velocity perturbation computed from (8). We still use an optimal scalar to minimize the cost function (10) by a step-length calculation on the extracted current velocity perturbation. We iterate until convergence.

Our approach helps the conventional FWI on convergence, especially at high frequencies. A good initial model is important. The high definition tomography (Guillaume et al., 2012) and conventional low frequency FWI can be used to build the initial model for our approach.

The importance of introducing a density or a pseudo-density term in FWI has been frequently highlighted (for example, Plessix et al., 2013). The fact that our formula (8) does not update the density model appears then as a possible drawback, partly mitigated by firstly the iterative process and secondly the possible use of a predefined velocity to density relationship (such as Gardner's law) as a constraint. The next challenge will be to introduce a density update into the inversion process (already introduced into ray-based approaches (Forgues and Lambaré, 1997), or even with the angle domain RTM (Zhang et al., 2014), which involves an amplitude versus angle (AVA) analysis.

Meanwhile, there is another potential application of our approach with much less penalization by density, i.e. FWI guided migration velocity analysis (MVA) (Allemand and Lambaré, 2014). In this approach the gradient of FWI is used as a guide for MVA. Since the cost function of MVA is driven only by kinematics, i.e. velocity, our improved FWI gradient appears well suited to replace the ray+Born inversion approximation currently used to guide this MVA. The benefit will be an improved accuracy of the guide, which is important given the heterogeneity of the velocity models normally estimated from FWI guided MVA.

Examples

To demonstrate the reliability and efficiency of our method compared with conventional FWI, we first apply our approach to the synthetic Marmousi II model (Martin et al., 2006). The model is simplified to a constant density isotropic acoustic model. The model is extended laterally and a 500 m thick water layer is added at the top. We show part of it in figure 1(a). The data are generated by finite difference modeling for a marine towed streamer acquisition with offsets ranging from 0 to 3 km. The source function is a Dirac function band-pass filtered within [3,60] Hz. Because every wave propagation program has its own numerical errors, we avoid using the same algorithm in the inversion process as used to simulate the synthetic data; therefore, we use the wave modeling tool from the SEISCOPE consortium to generate the data. High definition tomography is applied to obtain the initial model, figure 1(b). We start our FWI workflow at 4 Hz, a reasonable starting frequency in real data cases. We perform conventional FWI (Ratcliffe et al., 2013) updates in a 4 Hz to 11 Hz multi-scale inversion process. Six frequency ranges are defined and we use 6 iterations in each range. This conventional FWI iterates successfully to

DOI http://dx.doi.org/10.1190/segam2015-5865645.1

recover the model shown in figure 1(c), which is close to the true model in figure 1(a). For comparison, we perform our approach on the same frequency ranges in the FWI workflow, but with only 1 iteration in each frequency range. Figure 1(d) shows the result also using seismic data up to 11 Hz. Our approach has performed as well as conventional FWI, with higher resolution than the result in figure 1(c). The improved convergence is also confirmed by the more rapid decrease of the cost functions shown in figure 2(a). We compare three wells in detail in figure 2(b). The preserved amplitude RTM-based FWI matches the true model better than conventional FWI.

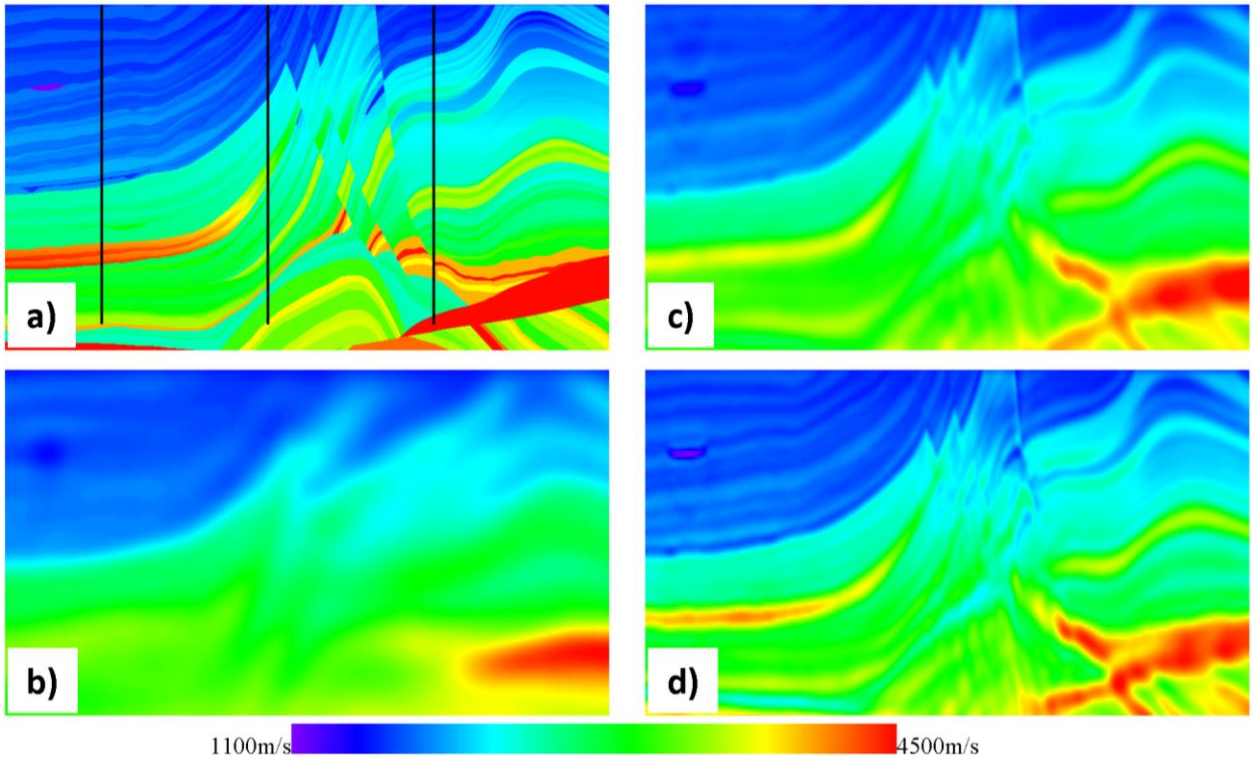

Figure 1: Test on Marmousi II model. *(a) The true model; (b) Initial model for FWI built from tomography; (c) 11 Hz conventional FWI result using 36 iterations in total; (d) 11 Hz preserved amplitude RTM-based FWI result using 6 iterations in total.*

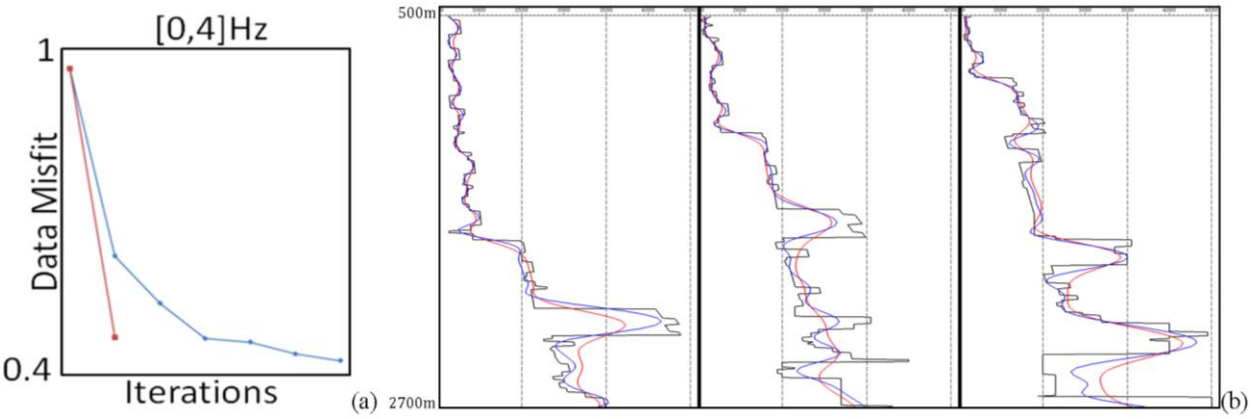

Figure 2: Test on Marmousi II model. *(a) Cost functions for the two tests on the first frequency range [0,4] Hz. 1 iteration of RTM-based FWI (red) converges as 3 iterations of conventional FWI (blue). (b) Detailed comparison between true model (black), conventional FWI (red) and RTM-based FWI (blue) at the three well locations indicated as the black lines on figure 1(a).*

DOI http://dx.doi.org/10.1190/segam2015-5865645.1

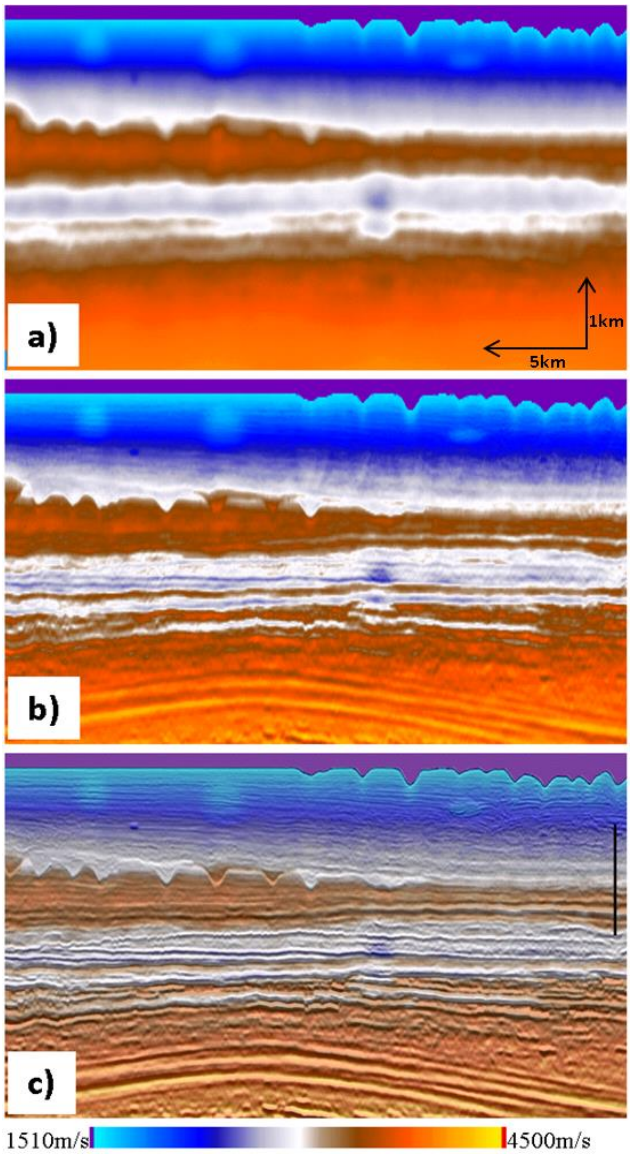

Figure 3: Test on Chevron/SEG dataset. *(a) Initial velocity model from tomography; (b) Preserved amplitude RTM-based FWI, only 2 iterations; (c) FWI overlaid with the corresponding PreSDM stack.*

In fact, given a reliable initial velocity model, we can use significantly less iterations to get a comparable result than the conventional FWI. To confirm this, we apply our approach to the Chevron/SEG 2014 FWI blind test dataset. The dataset consists of 1600 shot gathers with maximum offset of 8000 m. Conventional FWI can obtain an excellent result on this dataset with dozens of iterations (for example, Zhang et al., 2015). Here, to test our method, we build an initial model, figure 3(a), using ray-based tomography starting from the smooth initial velocity model provided by Chevron/SEG. It gives the lowest usable frequency in the seismic data. Then we perform only two iterations using shot domain preserved amplitude RTM, the first up to 10 Hz, the second up to 40 Hz. The result is shown in figure 3(b). Figure 3(c) shows excellent agreement between inverted velocity and the geological structure. Figure 4 shows the comparison with the well data that were provided with the dataset. The agreement is relatively good for only 2 iterations.

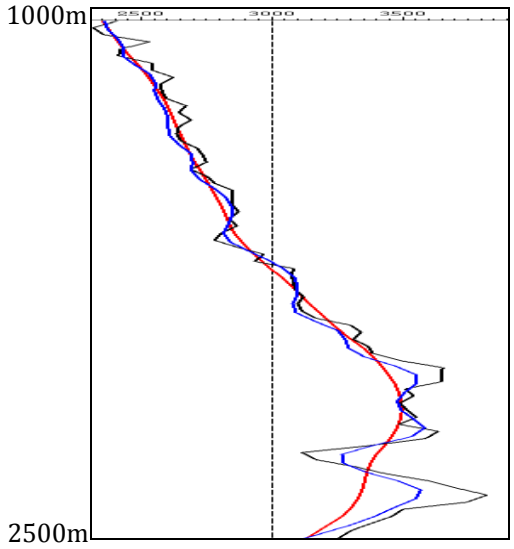

Figure 4: Test on Chevron/SEG dataset. *Comparison of well-log velocity (black), FWI velocity (blue) and the initial velocity from tomography (red). The well location is indicated as the black line on figure 3(c).*

Conclusions

We have developed a theory of shot domain preserved amplitude RTM to delineate the velocity perturbations of subsurface structures. Combined with the FWI iterative workflow, the method described here could be a useful tool to help conventional FWI for high resolution velocity model building from reflected waves. Examples have shown that the method is reliable and can provide faster convergence than conventional FWI.

Acknowledgements

We are grateful to Sam Gray, Andrew Ratcliffe, Leon Chernis and Yu Zhang for helpful discussions. We thank Andrew Ratcliffe and Ziqin Yu for the Chevron/SEG 2014 dataset preprocessing. We acknowledge Chevron and the SEG for providing the synthetic dataset, SEISCOPE for the wave modeling tool and CGG for the permission to publish this work.

DOI http://dx.doi.org/10.1190/segam2015-5865645.1

EDITED REFERENCES

Note: This reference list is a copyedited version of the reference list submitted by the author. Reference lists for the 2015 SEG Technical Program Expanded Abstracts have been copyedited so that references provided with the online metadata for each paper will achieve a high degree of linking to cited sources that appear on the Web.

REFERENCES

Allemand, T., and G. Lambaré, 2014, Full waveform inversion guided migration velocity analysis: 84th Annual International Meeting, SEG, Expanded Abstracts, 4712–4717.

Beylkin, G., 1985, Imaging of discontinuities in the inverse scattering problem by inversion of a causal generalized Radon transform: Journal of Mathematical Physics, **26**, no. 1, 99–108, http://dx.doi.org/10.1063/1.526755.

Bleistein, N., 1987, On the imaging of reflectors in the earth: Geophysics, **52**, 931–942, http://dx.doi.org/10.1190/1.1442363.

Bleistein, N., J. K. Cohen, and J. W. Stockwell, 2001, Mathematics of multidimensional seismic imaging, migration, and inversion: Springer-Verlag.

Duveneck, E., 2013, A pragmatic approach for computing full-volume RTM reflection angle/azimuth gathers: 75th Conference & Exhibition, EAGE, Extended Abstracts, doi:10.3997/2214-4609.20130472.

Forgues, E., and G. Lambaré, 1997, Parameterization study for acoustic and elastic ray plus Born inversion: Journal of Seismic Exploration, **6**, 253–277.

Guillaume, P., G. Lambaré, S. Sioni, X. Zhang, A. Prescott, D. Carotti, P. Dépré, S. Frehers, and H. Vosberg, 2012, Building detailed structurally conformable velocity models with high definition tomography: 74th Conference & Exhibition, EAGE, Extended Abstracts, W002, doi:10.3997/2214-4609.20148704.

Guitton, A., A. Valenciano, D. Bevc, and J. F. Claerbout, 2007, Smoothing imaging condition for shot profile migration: Geophysics, **72**, no. 3, S149–S154, http://dx.doi.org/10.1190/1.2712113.

Jin, S., R. Madariaga, J. Virieux, and G. Lambaré, 1992, Two-dimensional asymptotic iterative elastic inversion: Geophysical Journal International, **108**, no. 2, 575–588, http://dx.doi.org/10.1111/j.1365-246X.1992.tb04637.x.

Lailly, P., 1983, The seismic inverse problem as a sequence of before stack migrations: Proceedings of the Conference on Inverse Scattering — Theory and Application, SIAM, 206–220.

Martin, G. S., R. Wiley, and K. J. Marfurt, 2006, Marmousi 2: An elastic upgrade for Marmousi: The Leading Edge, **25**, 156–166, http://dx.doi.org/10.1190/1.2172306.

Plessix, R. E., P. Milcik, H. Rynja, A. Stopin, K. Matson, and S. Abri, 2013, Multiparameter full-waveform inversion: Marine and land examples: The Leading Edge, **32**, 1030–1038, http://dx.doi.org/10.1190/tle32091030.1.

Pratt, R. G., 1999, Seismic waveform inversion in the frequency domain, Part 1: Theory and verification in a physical scale model: Geophysics, **64**, 888–901, http://dx.doi.org/10.1190/1.1444597.

Ratcliffe, A., R. Jupp, R. Wombell, G. Body, V. Durussel, A. Fernandes, B. Gosling, and M. Lombardi, 2013, Full-waveform inversion of variable-depth streamer data: An application to shallow channel modeling in the North Sea: The Leading Edge, **32**, 1110–1115, http://dx.doi.org/10.1190/tle32091110.1.

DOI http://dx.doi.org/10.1190/segam2015-5865645.1

Tarantola, A., 1984, Inversion of seismic reflection data in the acoustic approximation: Geophysics, **49**, 1259–1266, http://dx.doi.org/10.1190/1.1441754.

Xu, S., Y. Zhang, and B. Tang, 2011, 3D angle gathers from reverse time migration: Geophysics, **76**, no. 2, S77–S92, http://dx.doi.org/10.1190/1.3536527.

Zhang, Y., A. Ratcliffe, G. Roberts, and L. Duan, 2014, Amplitude-preserving reverse time migration: From reflectivity to velocity and impedance inversion: Geophysics, **79**, no. 6, S271–S283, http://dx.doi.org/10.1190/geo2013-0460.1.

Zhang, Y., and J. Sun, 2009, Practical issues of reverse time migration: True amplitude gathers, noise removal and harmonic source encoding: First Break, **27**, no. 1, 53–59, doi:10.3997/1365-2397.2009002.

Zhang, Y., S. Xu, N. Bleistein, and G. Zhang, 2007, True-amplitude, angle-domain, common-image gathers from one-way wave-equation migrations: Geophysics, **72**, no. 1, S49–S58, http://dx.doi.org/10.1190/1.2399371.

DOI http://dx.doi.org/10.1190/segam2015-5865645.1